Geophys. J. Int. (2000) **143,** 809–820

Dynamic modelling of the subduction zone of central Mexico

A. Gardi,[1] M. Cocco,[2] A. M. Negredo,[1,*] R. Sabadini[1] and S. K. Singh[3]

[1] *Dipartimento di Scienze della Terra, Sezione Geofisica,Università di Milano, Italy. E-mail:annalisa.gardi@unimi.it*
[2] *Istituto Nazionale di Geofisica, Roma, Italy*
[3] *Instituto de Geofisica, UNAM, Mexico*

Accepted 2000 July 13. Received 2000 June 12; in original form 1999 July 15

SUMMARY

In central Mexico some significant normal faulting events have occurred within the subducted oceanic Cocos plate, just below or near the down-dip edge of the strongly coupled interface. These normal faulting shocks followed large shallow thrust earthquakes. In other subduction zones such events generally precede the up-dip thrust events. A vertical 2-D finite element modelling has been used to simulate the subduction of the Cocos plate beneath the North American plate when the slab is driven by an active convergence velocity or slab pull. We find that the latter mechanism plays only a minor role due to shallow subduction. The modelling results show that the stress pattern is very sensitive to the geometry of the plates. In particular, normal faulting earthquakes that follow large thrust events can be explained on the basis of the flexural response of the overriding and subducting plates to the peculiar geometry of this subduction zone, where the subducting slab becomes horizontal at about 100 km from the trench. This horizontal part of the subducting plate, down-dip with respect to the main thrust zone, is under an extensional stress field. This provides an alternative explanation to the slab pull for the occurrence of normal faulting intraplate earthquakes. In order for normal faulting earthquakes to occur in the early part of the seismic cycle, it is necessary that the large up-dip thrust events have a partial stress drop. We find that for small fractional stress drop, a wide region of extension remains below the down-dip edge of the main fault plane following a large thrust earthquake. Thus, the main thrust earthquakes do not invert the polarity of the active stress field, which is compressional and extensional up-dip and down-dip, respectively, with respect to the main thrust fault. Larger fractional stress drops result in larger delays in the occurrence of normal faulting events after the main thrust events.

Key words: earthquake cycle, Mexico, stress distribution, subduction.

1 INTRODUCTION

The subduction of the oceanic Cocos plate beneath the North American plate along the Middle American trench is characterized by a complex geometry of the downgoing slab. The dip angle of the subducting slab, the convergence rate (Molnar & Sykes 1969; Dean & Drake 1978; Burbach *et al.* 1984; DeMets *et al.* 1990; Ponce *et al.* 1992; Singh & Mortera 1992; Pardo & Suárez 1995) and the age of the Cocos plate (Klitgord & Mammerickx 1982; Singh & Mortera 1992; Kostoglodov & Ponce 1994; Pardo & Suárez 1995) vary along the Middle American Trench. Suárez *et al.* (1990), Singh & Pardo (1993) and Pardo & Suárez (1995) analysed the distribution of the seismicity. They used well-located earthquakes, based on local and teleseismic data, to constrain the geometry of the subducted plate in central Mexico. These authors concluded that the slab is not subducting at a constant angle, but it becomes almost subhorizontal after an initial low dip angle. Moreover, the Trans Mexican Volcanic Belt shows an unusual geometry, oblique with respect to the Middle American Trench (Fig. 1a). Under the assumption that volcanism is associated with the subduction process, this observation indicates a variable and complex geometry of the subducted plate.

The Mexican subduction zone is characterized by large thrust faulting earthquakes that occur at shallow depths (less than 25 km). Intraplate normal faulting earthquakes in the subducted plate generally occur down-dip at some distance from the strongly coupled interplate interface. However, in the central section of the Mexican subduction zone, significant normal faulting earthquakes also occur just below or near the down-dip edge of the coupled interface. Two recent examples are the

* Now at: Departamento de Geofisica, Universidad Complutense de Madrid, Spain.

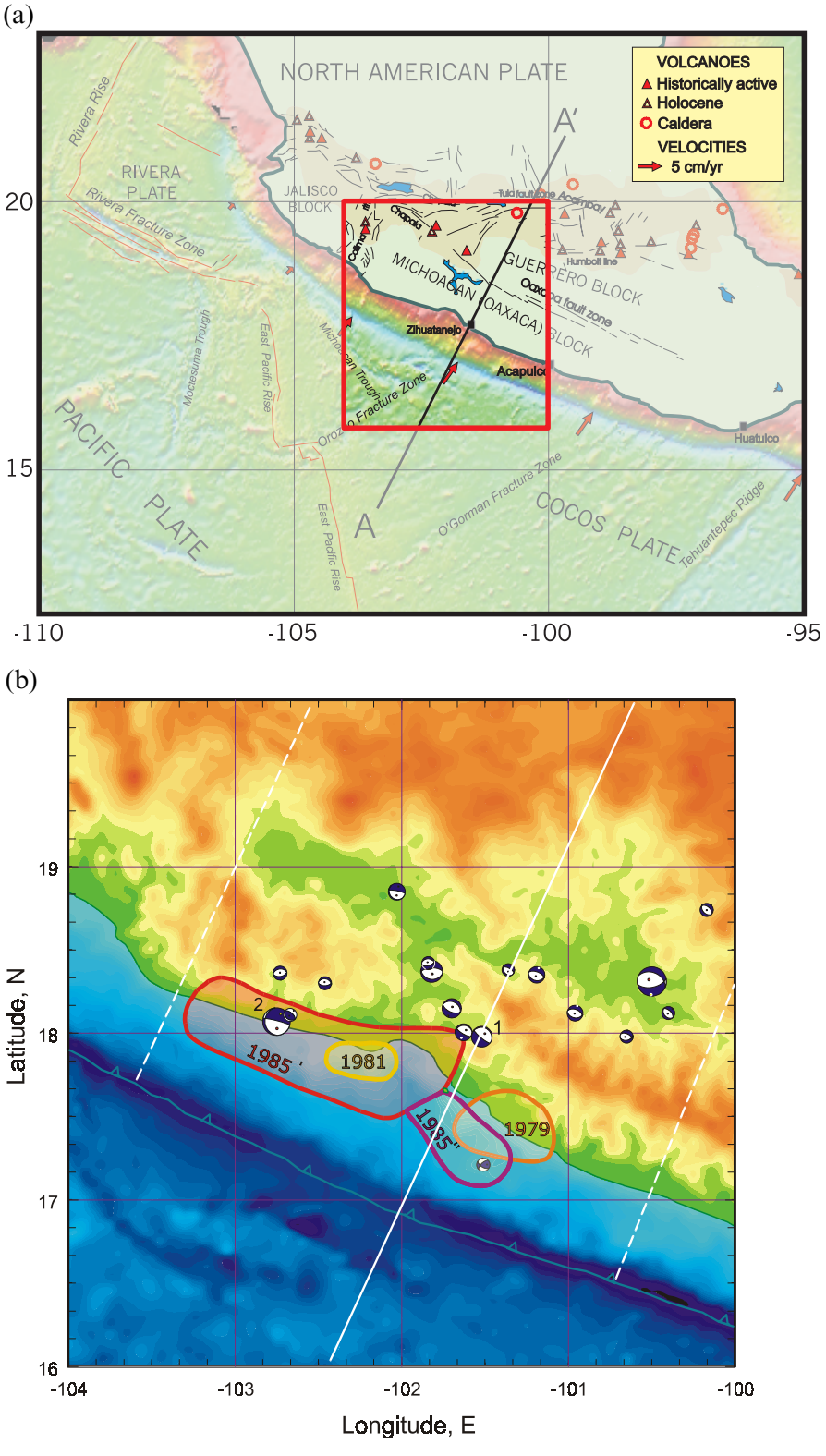

Figure 1. (a) Tectonic map of the region. The rectangle outlines the area of study. Line AA′ indicates the modelled vertical cross-section. (b) Intraplate events ($M_w \geq 5.4$; $H \geq 35$ km) in the subducted Cocos plate during 1964–1999 and their focal mechanisms. Only events in the area enclosed by the trench and the two parallel dashed lines have been considered. Rupture areas of large interplate thrust earthquakes, which occurred in the same time period, are shown by contours. Numbers 1 and 2 indicate the events of 1994 December 10 ($M_w = 6.6$; Cocco *et al.* 1997) and 1997 January 11 ($M_w = 7.1$; Mikumo *et al.* 1999), respectively. The solid white line indicates the orientation of our cross-section. (c) Vertical section perpendicular to the trench showing intraplate events and the rupture widths of interplate earthquakes. The origin is taken at the intersection of $-102°$E and the trench. Circles and dots: tensional and compressional axes within 30° of the dip of the slab (taken as 15°), respectively. X: oblique event that does not fulfil the above criteria or has a strike-slip mechanism. Sense of relative motions and rupture extents of events 1 and 2 are shown. Dashed line delineates the boundary between the plates.

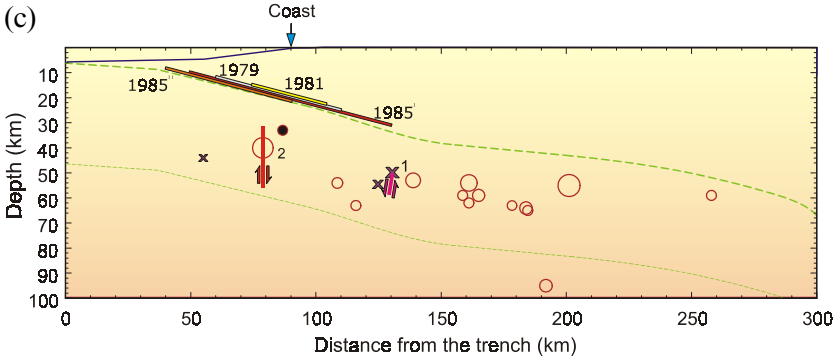

Figure 1. (*Continued.*)

earthquakes of 1994 December 10, $M_w = 6.6$ (Cocco *et al.* 1997), and 1997 January 11, $M_w = 7.1$ (Mikumo *et al.* 1999). Figs 1(b) and (c) show the locations of the events. It should be noted that these earthquakes took place in two different positions within the subducting plate and that the movement occurred in opposite directions along the two fault planes (see Fig. 1c), suggesting a very heterogeneous stress distribution in that portion of the slab. These earthquakes were preceded by large thrust events in 1979 ($M_w = 7.6$), 1981 ($M_w = 7.4$) and 1985 ($M_w = 8.0$, 7.6) that ruptured about 210 km of the plate interface in the region. The fact that the earthquakes of 1994 and 1997 were preceded by these large, shallow, low-angle thrust events is unusual in comparison with other subduction zones, where normal faulting events precede, not succeed, the up-dip large thrust events (Malgrange & Madariaga 1983; Astiz & Kanamori 1986; Dmowska *et al.* 1988; Lay *et al.* 1989). A similar observation has recently been presented for central Chile by Lemoine *et al.* (2000).

Cocco *et al.* (1997) suggested a causal relationship between the 1994 intermediate-depth normal faulting earthquake and the preceding shallow thrust events. From theoretical calculations, Mikumo *et al.* (1999) found evidence that the 1997 earthquake occurred in the subducted plate (see Figs 1b and c) in the region of maximum coseismic stress increase resulting from 1985 thrust earthquakes. However, a more complete understanding of the temporal and spatial distributions of normal faulting earthquakes in this part of the subducted Cocos plate is desirable.

Towards this goal, in this paper we investigate the state of stress within the subducted Cocos plate by using a 2-D finite element approach to model the stress distribution along vertical cross-sections perpendicular to the trench, focusing on the pattern of the stress field within the subducted plate. Although the complex tectonic setting of this area indicates that a complete approach would require a 3-D modelling, our study represents a first attempt to understand the mechanics controlling the seismic cycles of large and moderate-magnitude earthquakes better.

We model the stress accumulation process in the presence of locked seismogenic zones as well as the subsequent stress release caused by large thrust events. In other words, we investigate how periodic slip modulates the stress state within the subducted plate resulting from steady-state loading (see also Taylor *et al.* 1996, 1998; Dmowska *et al.* 1996; Zheng *et al.* 1996). Following Taylor *et al.* (1996), we refer to asperities as well as main thrust zones as regions of high moment release during large thrust earthquakes that are locked during the interseismic period. The influence of locked fault zones along subduction interfaces was first investigated in detail by Dmowska & Lovison (1988, 1992) and by Dmowska *et al.* (1996). These studies show that the locking of the seismogenic zone causes high stresses within the earthquake cycle that generate earthquakes that may be considered as intermediate-term precursors. This is opposite to the case of the normal faulting events that we investigate, since they occur after the large up-dip thrust earthquakes.

2 MODEL CHARACTERISTICS

The subduction of the oceanic Cocos plate beneath the North American plate is modelled by means of the finite element code MARC along a 2-D vertical cross-section (Fig. 1c). The scheme is a purely mechanical one, since the coupling between the momentum and temperature equations is not taken into account.

Four different geometries are considered following the results of recent studies in the area of central Mexico (Suárez *et al.* 1990; Singh & Pardo 1993; Pardo & Suárez 1995; Kostoglodov *et al.* 1996; Cocco *et al.* 1997). All geometries are characterized by vertical and horizontal extents of 600 and 1540 km, respectively (Fig. 2), in order to avoid border effects in the region of interest.

The trench corresponds to the origin of the horizontal scale (0 km). The western coast of Mexico is located about 90 km NE of the trench (along the profile shown in Fig. 1c), while the magmatic arc is located at 375 km. At depths of less than 30–40 km, the geometry of the subducted lithospheric plate is constrained by the hypocentral distribution, which indicates a dip angle between 10° and 25°. Unfortunately, the geometry of the slab as it deepens beneath the North American plate is poorly constrained and for this reason we have considered four different models, all characterized by shallow subduction. Seismic tomography results are inconclusive with respect to the depth reached by the subducted plate in central Mexico. Although there is indication of a high-velocity region in the mantle at depths of 300-400 km (Bijwaard *et al.* 1998), there is no evidence of continuity between this velocity anomaly and the seismogenic zone. For this reason, we have defined the geometry and the depth of the subducted plate on the basis of the hypocentral distribution of earthquakes.

Fig. 2(a) depicts the characteristics of the reference model M1, which has the simplest geometry. It provides a useful reference model and also corresponds to the Benioff zone in

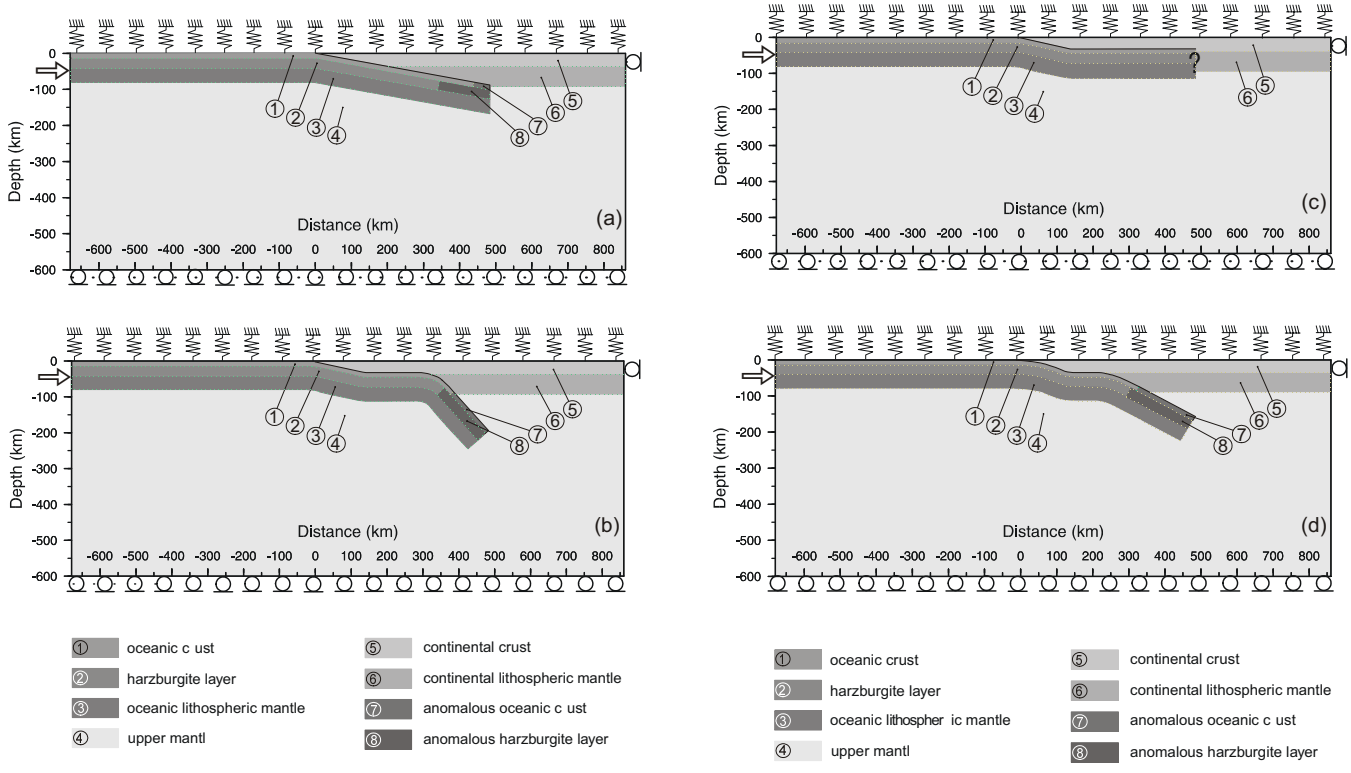

Figure 2. Geometry, materials and boundary conditions of the 2-D models M1 (a), M2 (b), M3 (c) and M4 (d). The circles indicate a free-slip condition. The spring symbols represent the buoyant restoring force applied at the upper surface. The white arrows on the top left denote the velocity applied in some calculations to simulate plate convergence.

southern Mexico (Singh *et al*. 1985; Pardo & Suárez 1995). The dip angle of the subducting lithosphere is about 10° and the bottom of the slab reaches a maximum depth of 166 km at about 485 km from the trench. Model M2, shown in Fig. 2(b), is based on Cocco *et al*. (1997). The initial dip angle of 12° is maintained as far as about 100 km from the trench, at which point the plate straightens out. At 250 km the oceanic lithosphere bends to 45° and starts its descent into the mantle, reaching a depth of about 80–90 km underneath the volcanic arc. In model M3 (Fig. 2c), based on Kostoglodov *et al*. (1996), the slab is flat after an initial bending. The oceanic plate plunges with the same dip angle as in the previous models (12°), flattening at 140 km. Although this geometry is unlikely, it has been considered for completeness and to understand better the effect of geometry on the stress distribution within the subducted plate. Finally, we consider model M4 (Fig. 2d), inferred from Pardo & Suárez (1995). In this model, which is similar to M2, the descending lithosphere is characterized by an initial dip of 4°, which becomes 23° at 75 km from the trench; the slab unbends to become horizontal and then plunges again with a dip angle of 30°.

We assume an earth stratification characterized by an oceanic lithosphere consisting of a basaltic oceanic crust (mid-ocean ridge basalt, MORB) 13 km thick, a harzburgite layer (Irifune & Ringwood 1987) 27 km thick and an oceanic lithospheric mantle of 50 km. The overriding plate is differentiated into a continental crustal layer of 35 km and a continental lithospheric mantle of 55 km. The earth stratification adopted is shown in Fig. 2. Our assumptions are consistent with those of other authors (Helsley *et al.* 1975; Couch & Woodcock 1981; Irifune & Ringwood 1987). The model is based on the viscoelastic Maxwell rheology, which accounts for the elastic behaviour of the lithosphere on short timescales and the long-term viscous behaviour. The viscosity of the crustal and harzburgitic layers is taken as 10^{24} Pa s, whereas for the lithospheric and asthenospheric mantle it is taken as 5×10^{22} and 10^{21} Pa s, respectively (Whittaker *et al*. 1992; Spada *et al*. 1992; Giunchi *et al*. 1996a,b). With this rheology a total time of at least 200 kyr is required by the models to lose their memory of the initial, unrealistic stress condition (Giunchi *et al*. 1996b). An elastic upper lithosphere has been considered in order to study the stick-slip behaviour because of the short timescale (nearly 250–300 yr) involved in the seismic cycle. During such a short time interval, the uppermost lithosphere can be considered perfectly elastic (Savage 1983; Thatcher & Rundle 1984; Whittaker *et al*. 1992). The model parameters for each layer are listed in Table 1.

The value of viscosity for the lithospheric mantle (5×10^{22} Pa s) has been selected in agreement with tectonic models for other similar regions (Whittaker *et al*. 1992; Giunchi *et al*. 1996a,b;

Table 1. Mechanical properties of the materials.

	Viscosity η (Pa s)	Poisson's ratio ν	Young's modulus E (Pa)
Oceanic crust + harzburgite	10^{24}	0.27	1.75×10^{11}
Continental crust	10^{24}	0.25	9×10^{10}
Lithospheric mantle	5×10^{22}	0.27	1.75×10^{11}
Asthenospheric mantle	10^{21}	0.27	1.75×10^{11}

Carminati *et al.* 1999) and with the estimate obtained by Houseman & Gubbins (1997). This value yields a relaxation time that is much larger than the loading periods investigated in this study. Therefore, the behaviour of the lithospheric mantle in our modelling can be considered as nearly elastic, consistent with the assumptions of Wahr & Wyss (1980) and Zheng *et al.* (1996). We have also tested our modelling results by using different values of the viscosity in the lithospheric mantle in the range 10^{20}–10^{22} Pa s. The tests show that our modelling results are modestly dependent on the viscosity values assumed. We will further discuss this issue later in the paper.

The following boundary conditions were applied to the whole set of models. The bottom of the grid is fixed in the vertical direction and the right side, from the surface to the depth of the lithosphere (90 km), is fixed in the horizontal direction. The other sides of the grid are free, allowing horizontal flow of the upper mantle material across the vertical boundaries. A gravity load is applied to all the elements of the meshes, with a value of 9.8 m s^{-2}. The isostatic restoring forces acting at the boundaries between density contrasts are taken into account using the Winkler foundation (Williams & Richardson 1991; Whittaker *et al.* 1992; Giunchi *et al.* 1996a,b). This procedure is based on the application at the boundary between different materials of a vertical force proportional to the density contrast and to the vertical displacement. For the sake of simplicity, this force is only applied where the density contrast is greatest, that is, to the upper free surfaces of the models.

To evaluate the slab pull effects, positive density contrasts of 130 and 20 kg m^{-3} are assigned to the MORB and harzburgitic layers, respectively (layers 7 and 8 in Fig. 2). These density anomalies, resulting from the phase transformation of a subducting oceanic plate when it exceeds a depth of about 90 km, are based on the petrological studies of Irifune & Ringwood (1987). Because the density anomalies are localized in these layers, the absolute density values of the materials are not relevant for this type of modelling. In order to simulate plate convergence of 5.5 cm yr^{-1}, the corresponding horizontal displacement is applied at each time step to the nodes of the Cocos lithospheric plate, at the left side of the grid.

The fault plane is obtained using the dual-node technique (Goodman *et al.* 1968; Whittaker *et al.* 1992) and movement along that plane is ensured by the assumption of a zero friction coefficient. Our modelling strategy consists of two different parts. We first consider a steady-state subduction (Savage 1983; Thatcher & Rundle 1984) characterized by a free-slip condition along the plate interface. In this case we simply specify the geometry of the plate boundary that slips depending on the applied driving forces. For each model we investigate the effect of free slip both when the slab is solely driven by the slab pull and when a convergence velocity is applied to the left side of the oceanic lithosphere as indicated by the arrows in Fig. 2. This configuration represents the stress and the deformation rate due to the forces that influence plate motion (see also Taylor *et al.* 1996) caused by density variations, long-term viscous flow in the mantle and plastic deformation within lithospheric plates.

After several tests, we restrict our analysis to the two more interesting geometries, M1 and M4, and study their behaviour during the locking and unlocking of the main thrust zone. We therefore investigate the stress fluctuations caused by the locking and unlocking of the main thrust zone. The seismogenic zone represents a fault zone that has large slip during periodic great earthquakes, but remains locked during the interseismic period. The locked condition is realized by impeding slip on the main thrust zone. We simulate the rupture of the main thrust zone assuming a zero friction coefficient and prescribing the amount of slip expected on the rupture plane as a boundary condition. The uniform displacement imposed to simulate the main thrust event is of 4 m, which is in reasonable agreement with the heterogeneous slip distribution obtained for the 1985 ($M_w = 8.0$) Michoacan earthquake by Mendoza & Hartzell (1988, 1989). It is important to point out that, following Savage (1983) and Thatcher & Rundle (1984), the total stress field is given by the superposition of a long-term steady-state stress field and periodic fluctuations caused by large thrust earthquakes (see also Taylor *et al.* 1996). However, the main difference between our modelling approach and that proposed by Savage (1983) is that we consider a true locked fault without applying any virtual dislocation. Therefore, the long-term and the earthquake-induced stress fields are not decoupled. Moreover, our numerical approach is a fully viscoelastic model, whereas Savage (1983) and Thatcher & Rundle (1984) considered a single viscoelastic layer with no slab penetration into the asthenosphere.

The pattern of the stress field is represented by means of the equivalent von Mises stress distribution, obtained from an equivalent intensity of the deviatoric stress tensor, defined as

$$\bar{\sigma} = \sqrt{\frac{3}{2} S_{ij} S_{ij}}\,, \tag{1}$$

$$S_{ij} = \sigma - \frac{1}{3}\,\delta_{ij}\sigma_{kk}\,, \tag{2}$$

where σ and S are the stress and deviatoric stress tensor, respectively. We prefer this representation of the stress field because it allows us to show the intensity of the stress tensor within the volume, without choosing a particular geometry of the plane as required by the Coulomb stress analysis. The principal stress axes have also been calculated, but in order to simplify the stress field representation only the axis with the major absolute eigenvalue is shown.

3 FREE-SLIP SIMULATION

We first present simulations corresponding to free slip between the overriding and descending plates, with slab pull being the active mechanism. Fig. 3(a) portrays the von Mises stress distribution calculated in the central part of model M1. This representation shows that the stress concentrates along the top of the subducting plate and at the free surface above the tip of the slab.

The stress concentration on the top of the slab is due to the stiff rheology of this part of the slab and to the bending moment caused by slab pull. The stress concentration at the free surface is related to the downwarping of the overriding plate at 450 km and represents the flexural response of the overriding plate to slab pull; this region corresponds to the volcanic arc. The level of stress is generally low, at most 40 MPa. Fig. 3(b), which shows the major principal stress axes for model M1, helps us to understand better the nature of the stress concentration within the top of the subducted slab. This part of the slab is in fact dominated by an extensional stress field caused by the flexural response to slab pull. In fact, the thin lines indicating tensional stresses are distributed within the whole uppermost oceanic plate. Tensional stresses are parallel

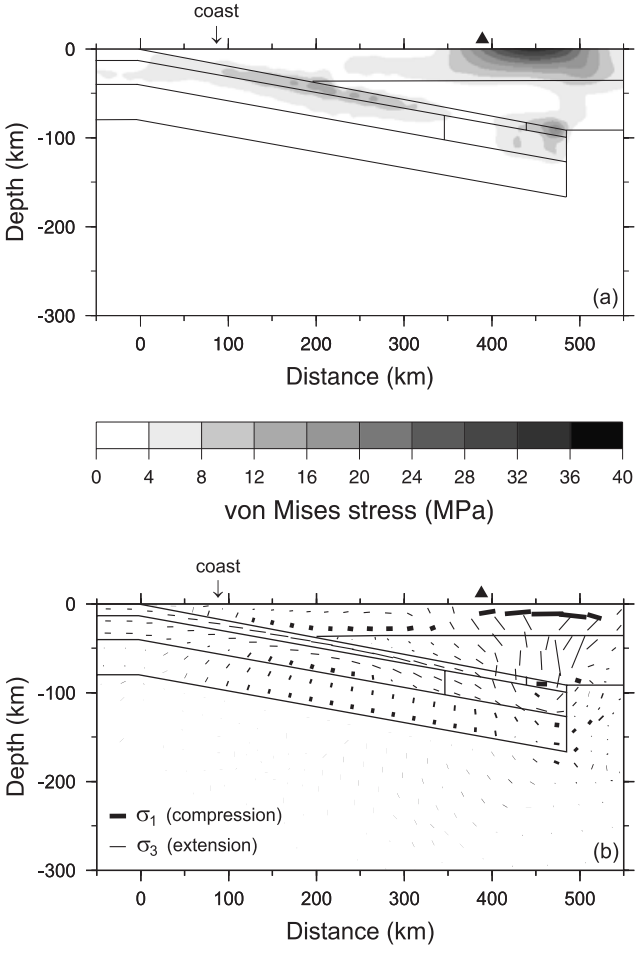

Figure 3. Results obtained with model M1 when free slip driven solely by slab pull is simulated. (a) Von Mises stress distribution in MPa. (b) Major principal stress axes, thick for compression and thin for extension. Eigenvector length is scaled to the eigenvalue. The black triangles give the position of the volcanic arc.

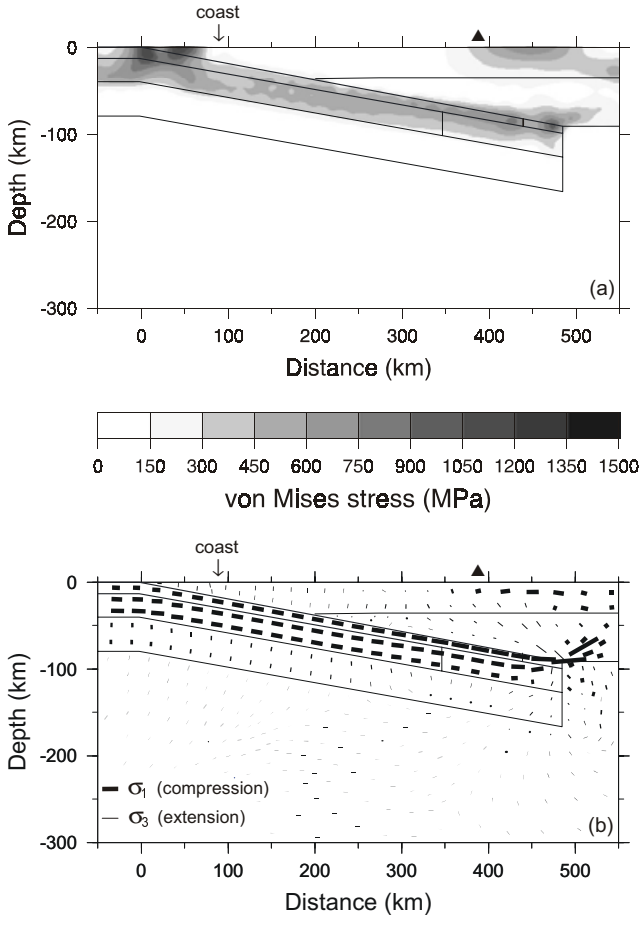

Figure 4. Results obtained with model M1 when free slip driven by a convergence rate of 5.5 cm yr^{-1} is simulated. Same representation as in Fig. 3.

to the dip of the slab, except in the proximity of the tip, where some amount of compressional stress is due to the geometry of the boundaries and does not have a real physical significance. Tension is distributed uniformly from the trench region to the tip due to the combination of relative free slip of the plates and slab pull. In the lowermost part of the slab, some amount of compression is also present, as expected for bending. A noteworthy feature of the stress pattern in the overriding plate is the vertical direction of the tensional stresses in the region above the tip of the slab due to the downpull of the subducting slab. In this region and in the proximity of the free surface, the horizontal compression is due to the downbending of the plate. A similar result is also obtained for models M2 and M4: the stress pattern continues to be characterized by tensional stresses in the uppermost part of the plate for varying plate geometries. Model M3 is not considered since the tip of the slab does not reach a depth appropriate for phase transformation.

Adding the high convergence velocity that characterizes the subduction in central Mexico, the simulations with model M1 gives rise to compressional stresses within the descending plate. Fig. 4(a) shows the von Mises stress distribution for this model. Because the plate convergence of 5.5 cm yr^{-1} is a consequence of both of slab pull and ridge push effects, we neglect the effect of the slab pull when applying this kinematic boundary condition.

The most striking difference with respect to Fig. 3(a) is the high level of stress for the case of active convergence, as indicated by the horizontal scale at the bottom of Fig. 4(a). With respect to the case of slab pull, the von Mises stress increases in the subducting plate from 20–24 MPa to 750–900 MPa. From a comparison of Figs 3(a) and 4(a), we note that in the latter case the von Mises stress is uniformly distributed in the whole uppermost part of the subducting plate. The lower level of stress in the deepest portion of the subducting plate is due to the reduced viscosity, which causes stress relaxation. In particular, a stress concentration occurs in the trench zone due to the push from the left, where the lithosphere starts to bend. The downbending of the overriding plate due to slab pull is reduced with respect to Fig. 3(a), since active convergence becomes the dominant mechanism. Fig. 4(b) shows the major principal stress axes calculated for model M1. With respect to Fig. 3(b), the style of stress in the uppermost subducting plate changes from extension to compression. Also, the extension in the overriding plate is drastically reduced with respect to Fig. 3(b), being limited to a small region in the proximity of the tip of the subducting plate; compression now dominates the overriding plate also due to active convergence.

We next consider model M4, which exhibits some interesting results (Fig. 5). The small dip angle at the surface (4°) produces an important upwelling of the overriding plate at a horizontal distance of 100 km, and the flexural response of the overriding and subducting plates to this upwelling causes tensional stresses in the upper portion of the subducted plate at a distance of about 150 km (Fig. 5b).

Compression due to convergence is not completely cancelled by this effect and is transmitted to the tip of the slab via the deepest horizontal portion of the subducted plate, between 150 and 250 km. This flexural effect due to the geometry could provide the explanation for the occurrence of normal faulting events such as that of Zihuatanejo in December 1994, whose hypocentre was located at a depth of about 50 km, exactly where the model predicts tensional stresses. Also, the direction of extension agrees with the fault plane solutions of this earthquake. Furthermore, of all the models explored in our study, M4 fits most accurately the topographic profile, as shown in Fig. 6, where the vertical displacements calculated with M4 predict two uplifted regions similar to the two topographic highs visible along the profile.

It is important to note, however, that the slab curvature (or the way of smoothing the bends) can significantly affect the stress pattern (see also Zheng *et al.* 1996). This means that although the stress pattern in Fig. 5 is plausible, it might not be accurate in detail.

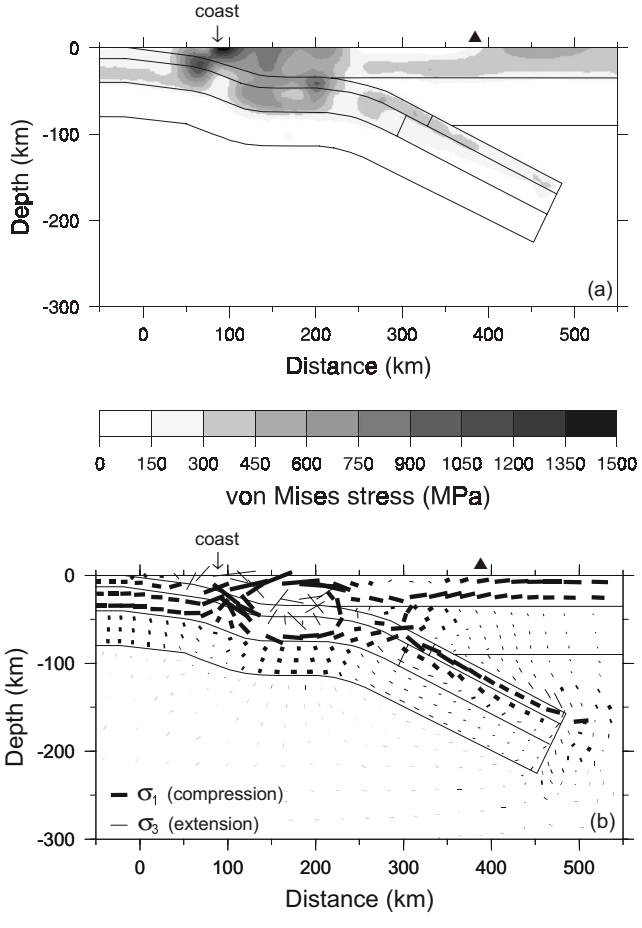

Figure 5. Results obtained with model M4 when free slip driven by the convergence rate is simulated. Same representation as in Fig. 3.

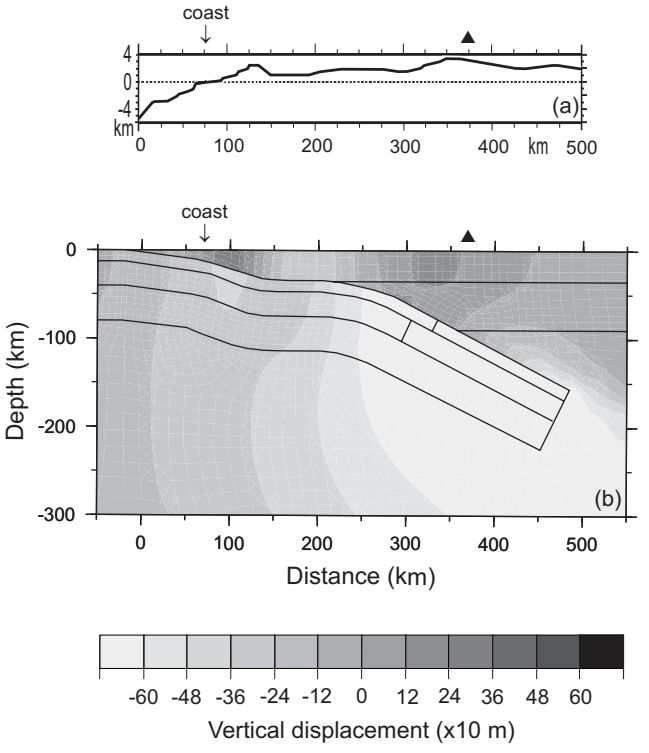

Figure 6. (a) Topographic profile of the study area. (b) Vertical displacements, in m, calculated with model M4 when free slip driven by the convergence rate is simulated.

The results of models M2 and M3 are not shown, being similar to those portrayed by M4 and M1, respectively. The different geometries of these models are responsible for minor modifications with respect to M4. With model M2 a higher concentration of stress is obtained at intermediate depths at the end of the horizontal portion of the slab where the push is counteracted by the overriding plate. Also, the pattern of the major stress axes of model M2 does not change significantly with respect to Fig. 4(b): there is a predominant compression within the descending plate. A small region of tensional stresses in the overriding plate remains in the proximity of the knee where the subducting slab plunges into the lithospheric mantle due to the drag produced by the subducting plate. When model M3 is considered with active convergence, we obtain a large stress concentration along the slab, as in model M2. The von Mises stress is mainly concentrated where the plate unbends to become horizontal and at the tip of the slab where there is an abrupt end of the fault plane. As in models M1 and M2, the major principal stress axes indicate a predominant compression within the oceanic lithosphere and tensional stresses within the continental plate located above the unbending point and above the tip of the descending slab.

Our model calculations thus show that during free-slip convergence, which accounts for the long-term behaviour of plate motion with the stick-slip behaviour averaged out, the stress pattern within the descending plate is strongly influenced by the bending and unbending of the slab and, in particular, by the dip angle and the width of the horizontal portion of the subducted plate. However, it is not influenced by the presence of slab pull, whose effect represents less than 10 per cent of the accumulated stress. Thus, the slab pull effect is negligible in our

results. This is due to the shallow subduction, which in our models is not deeper than 230 km. Such shallow subduction does not allow major phase changes to occur.

4 STICK-SLIP SIMULATION

Several tests with models M1 and M4 have been carried out to simulate the stick-slip behaviour of the plates. The tests consist of three steps: (1) the main thrust zone is locked and stress accumulation occurs due to plate convergence; (2) a displacement of 4 m is imposed along the main seismogenic zone to simulate the occurrence of a shallow thrust earthquake; and (3) the main thrust zone is locked again. Thus, a whole seismic cycle, as described by Dmowska *et al.* (1996) and Taylor *et al.* (1996), is investigated.

Fig. 7(a) displays the major principal stress axes calculated with model M1 after 200 yr, just before the earthquake. We note that this time interval is longer than the expected repeat time of large up-dip thrust earthquakes (Singh *et al.* 1981; Cocco *et al.* 1997). We consider this value as an upper bound for earthquake recurrence in the area of study. The important feature are the zones of compressional and extensional stresses located up-dip and down-dip of the locked part of the plate interface, respectively. The locked part is indicated by the thick grey segment in the figure. Compressional stresses are transmitted to the deepest part of the subducted lithosphere, in particular to the uppermost part of the lithosphere. This uppermost part of the lithosphere is stretched towards the tip of the slab and thus tensional stress accumulates below the down-dip edge of the locked interface. On the other hand, compressional stress develops in the whole lithosphere up-dip from the locked interface due to the high convergence rate and to the presence of the locked interface itself. This stress distribution is in agreement with what is generally expected in coupled subduction zones during an earthquake cycle (Dmowska *et al.* 1988; Taylor *et al.* 1996); in fact, in the last stage of a seismic cycle, before a large shallow thrust earthquake, normal faulting shocks occur in the deeper portion of the subducted plate. Examples of such a phenomenon have been reported for many zones around the world (Lay *et al.* 1989; Astiz *et al.* 1988), including central Mexico, where a normal faulting earthquake ($m_b = 5.2$) located in the subducted slab at about 100 km preceded the Michoacan events of 1985 by a few months (McNally *et al.* 1986). Furthermore, some reverse faulting shocks have been observed in the outer-rise zones (Dmowska & Lovison 1988), westwards of the trench, where our model correctly predicts compressional stresses.

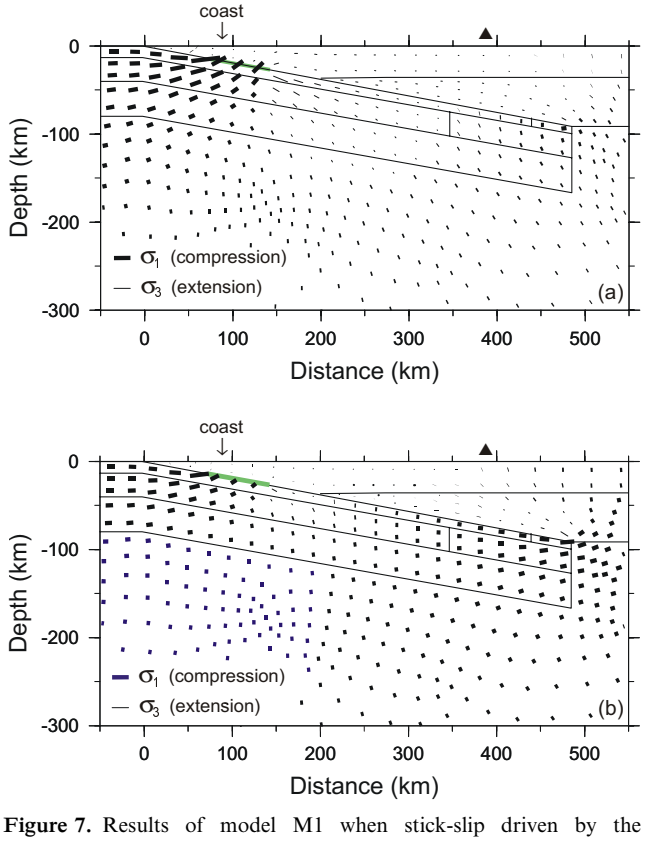

Figure 7. Results of model M1 when stick-slip driven by the convergence rate is simulated. The thick grey segment at the surface between the crust of the overriding plate and the subducted plate denotes the main thrust zone. (a) Major principal stress axes calculated at the end of a locking period of 200 yr. (b) Major principal stress axes calculated 10 yr after the large shallow thrust earthquake.

Fig. 7(b) depicts the major stress axes calculated 10 yr after the large shallow thrust earthquake. As a consequence of the stress released during the main shock, the thin vectors (extension) become shorter and the tensional stress zone is reduced in size because the compressional stress increases in the whole down-dip portion of the plate. This behaviour is consistent with the coseismic stress pattern change predicted for a thrust event by an elastic dislocation model: the coseismic rupture tends to increase the compression down-dip of the locked zone, thus inhibiting normal faulting events with nearly vertical fault planes, but it promotes them below the up-dip portion of the locked patch (see Mikumo *et al.* 1999). It is remarkable that, in our modelling, compressional stresses do not develop in the entire descending plate, indicating that the shock has not released all the accumulated stress. In fact, the displacement of 4 m provides a kinematic condition derived from seismic data recorded during the Michoacan event of 1985 September 19 ($M_w = 8.0$) but it does not necessarily correspond to the displacement that would be required to release the entire stress accumulated during a locking phase of 200 yr. It is also important to point out that a value of 4 m might not be typical of all the earthquakes in this segment of the slab.

Figs 7(a) and 8(a) show that the extension is well developed before the earthquake in both models M1 and M4. The most pronounced difference between these models is the size of the tensional stress region that remains after the large thrust earthquake (Fig. 8b). For the simple geometry of model M1, this region has a width of about 50 km and it is located around an average depth of about 35 km, whereas for model M4 a wider region of tensional stress (with a width of 120 km and reaching a maximum depth of 80 km) is obtained. This widening and deepening of the tensional stress zone is due to the flattening of the subducting slab, giving rise to a second knee within the plate that inhibits the motion of the plate itself. Therefore, normal faulting earthquakes can occur after the large up-dip thrust events due to the complex slab geometry. In both models M1 and M4 the tensional stress again increases below the down-dip edge of the fault plane when the main thrust zone is relocked. In other words, both the area and the amplitude of nearly horizontal extension increase with time after the large thrust event.

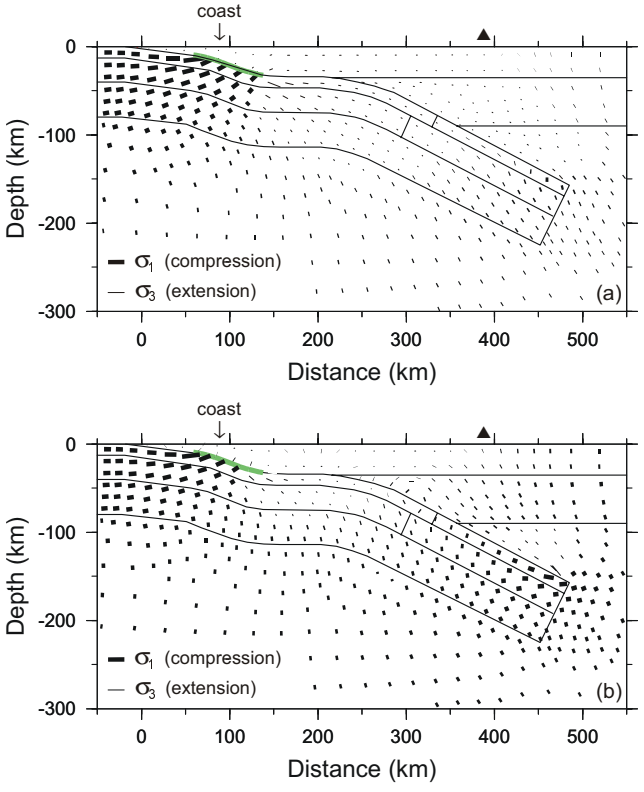

Figure 8. Results of model M4 when stick-slip driven by the convergence rate is simulated. Same representation as in Fig. 7.

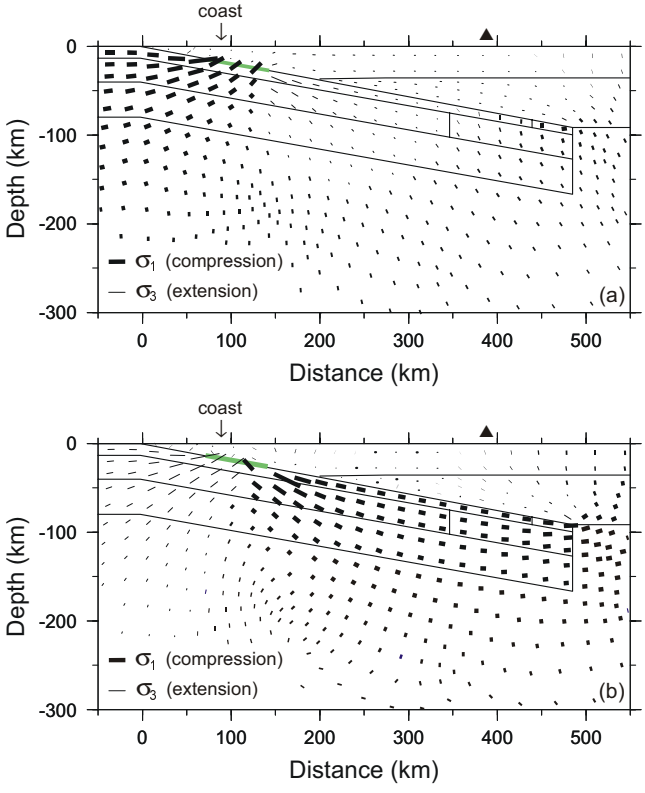

Figure 9. Results of model M1 when stick-slip driven by the convergence rate is simulated. (a) Major principal stress axes calculated at the end of a locking period of 40 yr. (b) Major principal stress axes calculated 10 yr after the thrust earthquake.

In order to understand better the competing effects on the stress perturbations caused by the coseismic rupture and the tectonic loading of the slab with a locked fault zone, we show in Fig. 9 the modelling results for the case when the locking period is only 40 yr and the coseismic slip is still 4 m. We show the simulations only for model M1, with M4 yielding similar results. This short recurrence time for large thrust earthquakes is likely to be a lower bound.

Reducing the loading period for the same coseismic slip during the thrust event corresponds to increasing the ratio between static stress drop and tectonic stress. This ratio can be considered as a fractional stress drop for the large up-dip thrust earthquakes. As an example, applying a plate convergence rate of 5.5 cm yr^{-1}, almost 70 yr is required for a complete stress drop if the coseismic slip is 4 m. Before the thrust earthquake the stress pattern (shown in Fig. 9a) is quite similar to that obtained with a locking period of 200 yr (Fig. 7a), although, as expected, smaller in amplitude. When the main thrust zone breaks with an imposed slip of 4 m, the coseismic stress drop is larger than that accumulated during the locking of the seismogenic zone (that is, fractional stress drop is larger than 1) and the deepest portion of the plate reverses the state of stress from tension (Fig. 9a) to compression (Fig. 9b). In other words, in this example, the coseismic stress changes instantaneously invert the stress pattern created by the plate convergence during the interseismic period in the presence of a locked seismogenic zone. This pattern is very similar to the coseismic stress changes obtained for the same zone by Mikumo *et al.* (1999). Under these circumstances a longer relocking period is required to restore extensional stress below the down-dip edge of the locked zone. Tensional stress begins to accumulate below the down-dip edge of the asperity only after a relocking period of about 150 yr. A similar result can be obtained by maintaining the same locking period and coseismic slip, but reducing the plate convergence. We have performed several tests using a convergence rate of 1 cm yr^{-1}. As expected, our modelling results indicate a trade-off between plate convergence velocity and the locking period of the seismogenic zone. High convergence rates yield persistent extensional stresses below the down-dip edge of the asperity, while large stress drops tend to invert such behaviour. We emphasize, however, that the plate convergence in the study area is better constrained than the repeat times of large thrust events.

5 DISCUSSION

The results presented above strongly depend on two assumptions: the period of time over which the main thrust zone has remained locked (that is, the repeat time of the large up-dip thrust events), and the amount of coseismic slip during the breaking of the seismogenic zone (that is, the static stress drop of the thrust earthquake). The slip value used in our simulation is the average (uniform) slip resulting from the seismic moment ($M_0 10^{28}$ dyn cm; see Mendoza & Hartzell 1988). We consider a fault area of 130×70 km^2 for large up-dip thrust events in the region. The assumed fault width is constrained by the distribution of aftershocks of the 1985 Michoacan earthquake (UNAM Seismology Group 1986), although Mendoza & Hartzell (1989) and Mikumo *et al.* (1999) used a larger value. Thus, the width of the 1985 rupture and the average coseismic slip are

somewhat uncertain. Moreover, we use two extreme values for the repeat times of large thrust up-dip earthquakes: 40 and 200 yr. These two extreme values allow us to study the role played by the coseismic stress change and the stress redistribution when the subducting plate is loaded with a locked seismogenic zone. A 200 yr period of loading for models M1 and M4 (Figs 7 and 8) represents the case in which the effect of tectonic loading dominates over the coseismic stress change. The results corresponding to a 40 yr loading period, shown in Fig. 9, represent just the opposite.

The modelling results show that for normal faulting events to occur after the occurrence of large thrust earthquakes and just below the down-dip part of the rupture plane (as in the case of the 1994 Zihuatanejo event; see Fig. 1c and Cocco *et al*. 1997), it is necessary that the coseismic rupture does not release all the accumulated stress (see Figs 7 and 8) or that the reloading period is long enough to restore extensional stresses below the down-dip edge of the locked surface. This result is consistent with Taylor *et al*. (1996), who showed that the extensional stress increases with time below the down-dip part of the main thrust zone. Although this mechanism predicts compressional stresses below the up-dip part of the thrust rupture zone (see Fig. 8b), we note that normal faulting events on nearly vertical planes (such as the 1997 earthquake; see Fig. 1c and Mikumo *et al.* 1999) can still occur as the stress field is characterized by oblique compressional and extensional stress directions (σ_1 and σ_3) both lying on the vertical plane used for our modelling (see Fig. 8). The occurrence of this event has been interpreted by Mikumo *et al*. (1999) in terms of coseismic stress redistribution. Our results are consistent with those of Taylor *et al*. (1996), which clearly show that extensional stresses decrease with time below the up-dip part of the thrust zone. We note, however, that the 1994 and 1997 normal faulting earthquakes are located in two different positions with respect to the main thrust rupture plane. We emphasize that while normal faulting events located below the up-dip edge of the thrust rupture plane (such as the 1997 earthquake shown in Fig. 1) are quite unusual, normal events at intermediate depths below the down-dip edge are much more frequent. In this portion of the slab normal faulting earthquakes also occur on oblique (not vertical) fault planes (see Fig. 1), indicating a nearly horizontal extensional stress field. We suggest that this is controlled by both the slab geometry and the tectonic loading of the locked thrust zone.

The stress pattern shown in Figs 7, 8 and 9 also depends on the viscoelastic relaxation of the lithospheric mantle. We have verified this effect by comparing numerical simulations with different values of mantle viscosity ranging between $10^{19} \div 10^{22}$ Pa s. A reduction of the viscosity of the lithospheric mantle leads to an increase in the reloading time required to restore extensional stresses within the subducting plate and below the down-dip part of the thrust plane. However, this effect strongly depends on the assumed slab geometry. In fact, the result shown in Fig. 8(b) for model M4 is still valid for a viscosity of 10^{20} Pa s for the lithospheric mantle, while the same is not true of Fig. 7(b). This further confirms that the slab geometry plays a dominant role in explaining the persistence of extensional stresses below the down-dip part of the main thrust zone.

Our results highlight several interesting features that have to be considered in order to model the spatio-temporal perturbation of the stress pattern properly. First, it is evident that the slab geometry strongly controls the stress evolution. This effect can be more relevant than the slab rheology for complex slab geometries and short timescales (≤ 100 yr). Moreover, the partitioning of tectonic loading between ridge push and slab pull largely controls the temporal evolution of the stress field. For a shallow subhorizontal slab it is likely that ridge push forces dominate the stress inside the subducting slab when a locked interface is present during the interseismic period. At the same time, large shallow thrust earthquakes perturb the state of stress within the slab (see Taylor *et al*. 1996, 1998; Mikumo *et al*. 1999; this study). It is important to emphasize that these two competing effects act at different timescales. While the coseismic stress changes depend on the earthquake stress drop, the temporal evolution of stress depends on the long-term tectonic loading and locking period. These two processes can separately explain the occurrence of the 1994 and 1997 normal faulting earthquakes. Moreover, these events occurred in two different zones of stress redistribution pattern (see Figs 1c, 8 and 9). The temporal evolution of extensional stresses in these two positions have opposite trends: while extension increases with time below the down-dip part of the main (locked) thrust zone, the opposite occurs below the up-dip part (see Fig. 8 and Taylor *et al*. 1996).

Our simulations suggest that plate convergence during the interseismic period, when the main thrust zone is locked, tends to diminish the extensional stress field generated below the up-dip portion of the rupture plane by the coseismic dislocation. The opposite occurs below the down-dip part of the locked seismogenic zone. Therefore, according to these results it is unlikely that extensional stresses will occur in both of these regions. However, this is true only if the whole width of the main thrust zone is locked. If the width of the thrust rupture plane is greater than that used in our simulations (70 km), as suggested by Mendoza & Hartzell (1989) and Mikumo *et al*. (1999), the shallower part (the upper half of the width) may slip aseismically. Under these mechanical conditions, only the deeper part of the main seismogenic zone may actually be locked. In this case, therefore, the tectonic forces will still create extension below the down-dip portion of the thrust rupture plane, but they will generate smaller compressional stresses below the up-dip zone. This may result, after the coseismic rupture, in extensional stresses over a wide area below the thrust rupture plane. This speculation requires further modelling to test whether it is tenable.

6 CONCLUSIONS

The normal faulting events in the Cocos plate that occurred just below the main rupture plane in the early part of the earthquake cycle can be explained by the particular geometry of the subducted slab. The stress distribution within a subducted plate, under the free-slip condition between the descending slab and the overlying plate, is strongly influenced by the slab geometry. With active convergence and for models M1, M2 and M3, the compressional stresses concentrate along the uppermost part of the slab and, in the overriding plate, above the tip of the slab. Large tensional stresses build up at intermediate depths for slab geometries peculiar to central Mexico, as seen in our model M4 (Fig. 5b). In this model, the oceanic lithosphere begins to plunge with a very small dip angle and at 135 km from the trench the slab unbends to become subhorizontal. Such a geometry generates flexural phenomena within

the plates that can cause intraplate normal faulting events due to bending stresses.

This might be a feasible explanation for poorly coupled subduction zones as well as for long-term plate behaviour. In subduction zones where the coupling is high, the presence of a locked interface and the seismic cycle of large thrust events need to be considered (Dmowska & Lovison 1988, 1992; Dmowska *et al*. 1988, 1996; Taylor *et al*. 1996). There is a competing effect between the stress redistribution caused by the tectonic load with a locked interface during the interseismic period and the coseismic stress changes caused by large thrust earthquakes. Our simulations indicate that in order to have normal faulting events after the large thrust earthquakes and just below the down-dip edge of their rupture plane (as in the case of the 1994 Zihuatanejo event; Cocco *et al*. 1997), it is necessary that the rupture does not release all the accumulated stress (see Figs 7 and 8). This means a partial stress drop for the large thrust events and implies a fractional stress drop of less than 1. The slab geometry can enhance these effects by increasing the amplitude and the depth distribution of the extensional stress field (see Fig. 8). If the fractional stress drop is less than 1, the coseismic stress drop does not cause an inversion of the stress field in the region below the down-dip edge of the rupture plane, which remains in an extensional stress state. Therefore, the persistence of an extensional stress field is a necessary condition to explain the occurrence of normal faulting earthquakes in the early part of the seismic cycle of the thrust events. Smaller fractional stress drops would require a shorter time span to recover the appropriate conditions for normal faulting. The earthquake cycle is determined by the repeat time T of the large shallow thrust events. Let t be the delay in time for the occurrence of the normal faulting event after the thrust earthquake. Thus, small fractional stress drops should result in small value of t/T, these two parameters being proportional to one other. On the other hand, if the fractional stress drop is larger than or close to 1, a relatively long time interval is needed to recover the state of tensional stress below the major thrust zone.

The explanation for normal faulting in terms of the flexural response to the geometry of the subduction zone does not exclude other possible mechanisms such as slab pull, which is enerally thought to be the cause of a permanent state of tension within the slab down-dip with respect to the large thrust zones. For the central Mexico subduction segment there is a difficulty with slab pull in that the slab is not sufficiently deep to generate substantial extension.

A better understanding of the seismic cycle and of how to discriminate among the different scenarios portrayed above could come from a precise knowledge of the recurrence times of the thrust earthquakes. Unfortunately, in this area the recurrence intervals of thrust earthquakes with magnitudes comparable to those of the Petatlan 1979 and Michoacan 1985 events ($M > 7$) are poorly known. In the same general region, large earthquake occurred in 1911 ($M = 7.9$), 1941 ($M = 7.6$) and 1943 ($M = 7.6$). The rupture areas of these earthquakes are not well defined (UNAM Seismology Group 1986). It is, therefore, not possible to define the recurrence time with precision and to compare it with the timing that results from our analysis. However, following Cocco *et al*. (1997) the normal faulting events in central Mexico such as the 1994 Zihuatanejo earthquake appear to have occurred in the early part of the earthquake cycle. According to our modelling results such behaviour may result from a partial stress drop during the large shallow up-dip thrust events. Our results suggest that in a highly coupled subduction zone the tectonic loading of the slab should recover the coseismic stress changes within a few years of the large thrust events. However, other information is needed to model the spatio-temporal evolution of the stress field completely.

ACKNOWLEDGMENTS

We are grateful to Harmen Bijwaard, Wim Spakman and E. Robert Engdahl for providing us with their tomographic images of central Mexico. We are obliged to V. Kostoglodov for generously providing us with some figures. We thank Raúl Madariaga for encouragement and valuable discussions and for his revision of the paper. We appreciate the efforts and the detailed revisions from an anonymous referee.

REFERENCES

Astiz, L. & Kanamori, H., 1986. Interplate coupling and temporal variation of mechanisms of intermediate-depth earthquakes in Chile, *Bull. seism. Soc. Am.,* **76,** 1614–1622.

Astiz, L., Lay, T. & Kanamori, H., 1988. Large intermediate depth earthquakes and the subduction process, *Phys. Earth planet. Inter.,* **53,** 80–166.

Bijwaard, H., Spakman, W. & Engdahl, E.R., 1998. Closing the gap between regional and global travel time tomography, *J. geophys. Res.,* **103,** 30 055–30 078.

Burbach, G., Frolich, C., Pennington, W. & Matumoto, T., 1984. Seismicity and tectonics of the subducted Cocos plate, *J. geophys. Res.,* **89,** 7719–7735.

Carminati, E., Giunchi, C., Argnani, A., Sabadini, R. & Fernandez, M., 1999. Plio-Quaternary vertical motion of the Northern Apennines: insights from dynamic modelling, *Tectonics,* **18,** 703–718.

Cocco, M., Pacheco, J., Singh, S.K. & Courboulex, F., 1997. The Zihuatanejo, Mexico earthquake of 1994 December 10 ($M = 6, 6$): source characteristics and tectonic implications, *Geophys. J. Int.,* **131,** 135–145.

Couch, R. & Woodcock, S., 1981. Gravity and structure of the continental margins of southwestern Mexico and northwestern Guatemala, *J. geophys. Res.,* **86,** 1829–1840.

Dean, B.W. & Drake, C.L., 1978. Focal mechanism solutions and tectonics of the Middle America arc, *J. Geol.,* **86,** 111–128.

DeMets, C., Gordon, R.G., Argus, D.F. & Stein, S., 1990. Current plate motions, *Geophys. J. Int.,* **101,** 425–478.

Dmowska, R. & Lovison, L.C., 1988. Intermediate-term seismic precursors for some coupled subduction zones, *Pageoph,* **126,** 643–664.

Dmowska, R. & Lovison, L.C., 1992. Influence of asperities along subduction interfaces on the stressing and seismicity of adjacent areas, *Tectonophysics,* **211,** 23–43.

Dmowska, R., Rice, J.R., Lovison, L.C. & Josell, D., 1988. Stress transfer and seismic phenomena in coupled subduction zones during the earthquake cycle, *J. geophys. Res.,* **93,** 7869–7884.

Dmowska, R., Zheng, G. & Rice, J.R., 1996. Seismicity and deformation at convergent margins due to heterogeneous coupling, *J. geophys. Res.,* **101,** 3015–3029.

Giunchi, C., Kiratzi, A., Sabadini, R. & Louvari, E., 1996. A numerical model of the Hellenic subduction zone: active stress field and sea-level changes, *Geophys. Res. Lett.,* **23,** 2485–2488.

Giunchi, C., Sabadini, R., Boschi, E. & Gasperini, P., 1996. Dynamic models of subduction: geophysical and geological evidence in the Tyrrhenian Sea, *Geophys. J. Int.,* **126,** 555–578.

Goodman, R.E., Taylor, R.L. & Brekke, T.L., 1968. A model for the mechanics of jointed rock, *J. Soil Mech. Found. Div. Am. Soc. Civ. Eng.,* **94,** 637–658.

Helsley, C.E., Nation, J.B. & Meyer, R.B., 1975. Seismic refraction observations in southern Mexico (abstract), *EOS, Trans. Am. geophys. Un.,* **56,** 452.

Houseman, G. & Gubbins, D., 1997. Deformation and subducted oceanic lithosphere, *Geophys. J. Int.,* **131,** 535–551.

Irifune, T. & Ringwood, A.E., 1987. Phase transformations in a harzburgite composition to 26 GPa: implications for dynamical behaviour of the subducting slab, *Earth planet. Sci. Lett.,* **86,** 365–376.

Klitgord, K. & Mammerickx, J., 1982. East Pacific rise: magnetic anomaly and bathymetric framework, *J. geophys. Res.,* **87,** 6725–6750.

Kostoglodov, V. & Ponce, L., 1994. Relationship between subduction and seismicity in the Mexican part of the Middle America trench, *J. geophys. Res.,* **99,** 729–742.

Kostoglodov, V.,Bandy, W.,Domínguez, J. & Mena, M., 1996. Gravity and seismicity over the Guerrero seismic gap, *Geophys. Res. Lett.,* **23,** 3385–3388.

Lay, T., Astiz, L., Kanamori, H. & Christensen, D.H., 1989. Temporal variation of large intraplate earthquakes in coupled subduction zones, *Phys. Earth planet. Inter.,* **54,** 258–312.

Lemoine, A., Campos, J. & Madariaga, R., 2000. Evidence of earthquake interaction in the Illapel gap in central Chile: the July 1997—September 1998 sequence, *Geophys. Res. Lett.,* submitted.

Malgrange, M. & Madariaga, R., 1983. Complex distribution of large thrust and normal-fault earthquakes in the Chilean subduction zone, *Geophys. J. R. astr. Soc.,* **73,** 489–505.

McNally, K.C., Gonzalez-Ruiz, J.R. & Stolte, C., 1986. Seismogenesis of the 1985 great (Mw = 8.1) Michoacan, Mexico earthquake, *Geophys. Res. Lett.,* **13,** 585–588.

Mendoza, C. & Hartzell, S.H., 1988. Inversion for slip distribution using teleseismic P waveforms: North Palm Springs, Borah Peak and Michoacan earthquakes, *Bull. seism. Soc. Am.,* **78,** 1092–1111.

Mendoza, C. & Hartzell, S.H., 1989. Slip distribution of the 19 September 1985 Michoacan, Mexico, earthquake: near-source and teleseismic constraints, *Bull. seism. Soc. Am.,* **79,** 655–669.

Mikumo, T., Singh, S.K. & Santoyo, M.A., 1999. A possible stress interaction between large thrust and normal faulting earthquakes in the Mexican subduction zone, *Bull. seism. Soc. Am.,* **89,** 1418–1427.

Molnar, P. & Sykes, L.R., 1969. Tectonics of the Caribbean and Middle American region from focal mechanisms and seismicity, *Geol. Soc. Am. Bull.,* **80,** 1639–1684.

Pardo, M. & Suárez, G., 1995. Shape of the subducted Rivera and Cocos plates in southern Mexico: seismic and tectonic implications, *J. geophys. Res.,* **100,** 12 357–12 373.

Ponce, L., Gaulon, R., Suárez, G. & Lomas, E., 1992. Geometry and state of stress of the downgoing Cocos plate in the Isthmus of Tehuantepec, Mexico, *Geophys. Res. Lett.,* **19,** 773–776.

Savage, J.C., 1983. A dislocation model of strain accumulation and release at a subduction zone, *J. geophys. Res.,* **88,** 4984–4996.

Singh, S.K. & Mortera, F., 1992. Source-time functions of large Mexican subduction earthquakes, morphology of the Benioff zone and the extent of the Guerrero gap, *J. geophys. Res.,* **96,** 21 487–21 502.

Singh, S.K. & Pardo, M., 1993. Geometry of the Benioff zone and state of stress in the overriding plate in Central Mexico, *Geophys. Res. Lett.,* **20,** 1483–1486.

Singh, S.K., Havskov, J. & Astiz, L., 1981. Seismic gaps and recurrence periods of large earthquakes along the Mexican subduction zone: a reexamination, *Bull. seism. Soc. Am.,* **71,** 827–843.

Singh, S.K., Suárez, G. & Domínguez, T., 1985. The great Oaxaca earthquake of 15 January 1931: lithospheric normal faulting in the subducted Cocos plate, *Nature,* **317,** 56–58.

Spada, G., Ricard, Y. & Sabadini, R., 1992. Excitation of true polar wander by subduction, *Nature,* **360,** 452–454.

Suárez, G., Monfret, T., Wittlinger, G. & David, C., 1990. Geometry of subduction and depth of the seismogenic zone in the Guerrero gap, Mexico, *Nature,* **345,** 336–338.

Taylor, M.A.J., Zheng, G., Rice, J.R., Stuart, W.D. & Dmowska, R., 1996. Cyclic stressing and seismicity at strongly coupled subduction zones, *J. geophys. Res.,* **101,** 8363–8381.

Taylor, M.A.J., Dmowska, R. & Rice, J.R., 1998. Upper plate stressing and seismicity in the subduction earthquake cycle, *J. geophys. Res.,* **103,** 24 523–24 542.

Thatcher, W. & Rundle, J.B., 1984. A viscoelastic coupling model for the cyclic deformation due to periodically repeated earthquakes at subduction zones, *J. geophys. Res.,* **89,** 7631–7640.

UNAM Seismology Group, 1986. The September 1985 Michoacan earthquakes: aftershock distribution and history of rupture, *Geophys. Res. Lett.,* **13,** 573–576.

Wahr, J. & Wyss, M., 1980. Interpretation of coseismic deformation with a viscoelastic relaxation model, *J. geophys. Res.,* **85,** 6471–6477.

Whittaker, A., Bott, M.H.P. & Waghorn, G.D., 1992. Stresses and plate boundary forces associated with subduction plate margins, *J. geophys. Res.,* **97,** 11 933–11 944.

Williams, C.A. & Richardson, R.M., 1991. A rheologically layered three-dimensional model of the San Andreas fault in central and southern California, *J. geophys. Res.,* **96,** 16 597–16 623.

Zheng, G., Dmowska, R. & Rice, J.R., 1996. Modeling earthquake cycles in the Shumagin subduction segment, Alaska, with seismic and geodetic constraints, *J. geophys. Res.,* **101,** 8383–8392.